

Optical analysis of lens-like $\text{Cu}_2\text{CdSnS}_4$ quaternary alloy nanostructures

Ali Abu Odeh¹ · Y. Al-Douri^{1,2} · R. M. Ayub¹ · M. Ameri³ · A. Bouhemadou⁴ · Deo Prakash⁵ · K. D. Verma⁶

Received: 3 July 2016 / Accepted: 2 September 2016 / Published online: 13 September 2016
© Springer-Verlag Berlin Heidelberg 2016

Abstract $\text{Cu}_2\text{CdSnS}_4$ quaternary alloy nanostructures with different copper concentrations (0.2, 0.4, 0.6, 0.8 and 1.0 M) were successfully synthesized on n-type silicon substrates using spin coating technique with annealing temperature at 300 °C. Optical properties were analyzed through UV–Vis and Photoluminescence spectroscopies, and thus, there is a change in energy band gap with increasing Cu concentration from 0.2 to 1.0 M. The structural properties of $\text{Cu}_2\text{CdSnS}_4$ quaternary alloy nanostructures were investigated by X-ray diffraction. The particles size and shape have a direct relationship with copper concentration. Morphological and topographical studies were carried out by using scanning electron microscopy and atomic force microscopy. The obtained results are investigated to be available in the literature for future studies.

1 Introduction

Cu-III-IV-VI_4 and $\text{Cu}_2\text{-II-IV-VI}_4$ quaternary alloys (II = Zn, Cd; III = Ga, In; IV = Ge, Sn; VI = S, Se, Te) are known to have a potential for photovoltaic (PV) applications, light-emitting diodes and nonlinear optical devices [1], and these alloys are crystallized usually as a chalcopyrite-like (tetragonal or cubic) structure [2]. The industry of photovoltaic solar modules has grown rapidly during the last decades [3], and 80–90 % of the solar cell technology is dominated by silicon-based materials that is proved to be a solid technology in the PV modules due to the cheap price and abundance of the used silicon in bulk (first generation), thin film (second generation) and some of the nanostructured (third generation) solar cells [4]. Advancements in the area of concentrating photovoltaic (CPV) lead to a highest solar energy-to-electricity conversion efficiency [5], and also other investigations in perovskite photovoltaics revealed the exceptional light-absorbing properties exhibited by organometallic halides which are chemical compounds that contain bonds between organic compounds and metal [6].

The contribution of thin film PV technologies such as cadmium telluride (CdTe) and copper indium gallium selenide (CIGS) is increasing rapidly as the most promising solar cell technologies due to outstanding performance for optical and electronic devices [7, 8]. However, the limitations associated with the availability of raw materials and with the toxicity of some of them are likely to restrict further growth of these technologies [9, 10]. In CIGSSe devices, the indium-to-gallium ratio is used to control the band gap. Also, in CZTSSe devices, films should be both copper-poor and zinc-rich to form the highest performing devices [11]. On the other hand, CZTS/CdS solar cell device that fabricated by Dhakal et al. [12] using co-

✉ Y. Al-Douri
yaldouri@yahoo.com

¹ Institute of Nano Electronic Engineering, University Malaysia Perlis, 01000 Kangar, Perlis, Malaysia

² Physics Department, Faculty of Science, University of Sidi-Bel-Abbes, 22000 Sidi-Bel-Abbès, Algeria

³ Laboratoire Physico-Chimie des Matériaux Avancés (LPCMA), Université Djilali Liabès de Sidi Bel-Abbès, 22000 Sidi-Bel-Abbès, Algeria

⁴ Laboratory for Developing New Materials and Their Characterization, University of Setif 1, 19000 Sétif, Algeria

⁵ Faculty of Engineering, School of Computer Science and Engineering, SMVD University, Kakryal, Katra, J&K 182320, India

⁶ Material Science Research Laboratory, Department of Physics, S. V. College, Aligarh, U.P. 202001, India

sputtering technique followed by H₂S annealing is an excellent absorber because of its high absorption coefficient and its ideal band gap with 6.2 % efficient. The CZTS films showed a kesterite phase [13, 14].

It is well known that Cu₂CdSnS₄ (CCTS) quaternary alloy nanostructures crystallizes in a stannite (space group: I $\bar{4}$ 2m) structure [15]. Guo et al. [16] have synthesized Cu₂CdSnS₄ quaternary alloy using co-sputtering deposition, the estimated band gap value is about 1.4 eV and the structural analysis revealed the existence of 13 peaks in the tetragonal crystal structure with lattice parameters $a = 5.487 \text{ \AA}$ and $c = 10.845 \text{ \AA}$. CCTS semiconductor thin films were successfully deposited on glass via the chemical spray pyrolysis technique within a wide substrate temperature range from 250 to 500 °C. Xiao et al. [17] have synthesized Cu₂Cd_xZn_{1-x}SnS₄ alloy thin film with different Cd contents and single kesterite phase using the sol-gel method. Optical absorption measurements indicate that the band gap can be continuously tuned in a range of 1.55–1.09 eV as Cd concentration varied from $x = 0$ to 1, and hall effect measurements suggest that the hole concentration of CCZTS films decreases with increasing Cd concentration. Furthermore, the band gap of the kesterite CCZTS alloy decreases monotonically with increasing Cd concentration. Also, the same quaternary alloy nanofibres with different Cd concentrations were grown on glass substrate using the electrospinning technique by Ibrahim et al. [18], and optical measurements revealed a decrease in band gap from 1.75 to 1.61 eV, with the increasing Cd concentration from $x = 0$ to $x = 1$. Current-voltage measurements showed a power conversion efficiency of 3 % under the solar illumination with intensity of 100 mW/cm², and the lattice constants were 5.339 and 11.389 Å for a and c , respectively.

In this work, Cu₂CdSnS₄ quaternary alloy nanostructures with different copper concentrations were deposited via spin coating technique on n-type silicon substrate at annealing temperature, 300 °C. Optical (UV-Vis and PL), structural (XRD), morphological (SEM) and topographical (AFM) properties were investigated in detail, and the optimum Cu concentration for PV applications was determined. This paper is organized as follows: The next section details the experimental procedure, whereas Sect. 3 discusses the results and findings. Finally, conclusion is summarized in Sect. 4.

2 Experimental

All the chemicals and solvents that used were analytically graded and obtained from Sigma-Aldrich Company, and Cu₂CdSnS₄ quaternary alloy nanostructures were deposited

onto n-type silicon substrate using spin coating technique. The precursor's solutions were prepared from copper chloride (CuCl₂), cadmium chloride (CdCl₂) (0.8 M), tin chloride (SnCl₂) (0.8 M), thiourea (CH₄N₂S) (0.8 M), 2-methoxyethanol (2-metho) and monoethanolamine (MEA). The solvent and stabilizer were the 2-metho and MEA, respectively. The molar ratio of Cu, Cd, Sn and S in the solution was 2:1:1:4. To obtain the solutions with different copper (Cu) concentrations, the concentration of Cu was varied to give the values of 0.2, 0.4, 0.6, 0.8 and 1 M by using the following equations:

$$\text{Molarity } (M) = \frac{M_s}{V} \quad (1)$$

$$M_s = \frac{W \text{ (gm)}}{M_{wt} \text{ (gm/mol)}} \quad (2)$$

where M_s is number of moles, V is liquid volume, W is weight (gm) and M_{wt} is molecular weight (gm/mol). The mixing process of the precursors was done using a magnetic stirrer (WiseStir MSH 30D, Germany) for 3 h with a stirring speed of 1500 revolution per minute (RPM) at a temperature, 50 °C to completely dissolve the metals during stirring, which results in a yellow and transparent solution. Five solutions have been prepared at different copper concentrations (0.2, 0.4, 0.6, 0.8 and 1 M), each one has been divided into two parts equally, first is used in the deposition process without change and the second has been covered with laboratory film and placed inside ultrasonic cleaner (DELTA DC200H, Taiwan) that filled with deionized water at 50 °C for 30 min. Finally, two solutions are resulted for every copper concentration, one of them is with ultrasonic and the other is without ultrasonic.

A few drops of the resulting solutions—with and without ultrasonic—were dropped by using plastic dropper onto a separate n-type silicon substrate. A spin coater (Laurell WS-400B, USA) has been used at a rotation speed of 1500 RPM for 30 s for depositing the solution on the substrate, followed by drying the substrate at 80 °C for 1 min on a hot plate. The spin coating and drying processes were repeated 15 times for all the substrates to obtain a uniform nanostructures layer with a proper thickness on the top of the silicon substrate. As a result, ten samples have been prepared, five are with ultrasonic and the other five are without ultrasonic at different copper concentrations.

Annealing was applied to the samples by using a diffusion furnace (MODU-LAB, USA). All the samples have been annealed at 300 °C for 1 h under the flow of nitrogen gas N₂ to keep the deposited nanostructures coherent, and then, the samples were cooled below 40 °C. The optical properties have been tested by UV-Vis spectrometer (PerkinElmer Lambda 35, USA). The reflection spectra of the Cu₂CdSnS₄ quaternary alloy nanostructures were

recorded over the wavelength range 200–1000 nm. Also, energy band gap has been tested by using photoluminescence (PL) (Fluorolog-3, USA), and a wavelength range between 200 and 1100 nm has been selected.

The structural properties of Cu₂CdSnS₄ quaternary alloy nanostructures have been investigated by using X-ray diffractometer (Philips PW 1710, USA), which record the intensity as a function of Bragg's angle in 2θ range from 10° to 60° at a rate of 10°/min using Cu $\kappa\alpha$ ($\lambda = 1.5406 \text{ \AA}$). The major diffraction peaks have been recorded and attributed to the corresponding planes. The surface morphology was investigated by using scanning electron microscopy (SEM JSM-6010LV, Japan). The topography of the quaternary alloy was characterized by atomic force microscopy (AFM) (SPA 400, Seiko Instruments Inc., Japan) with a scanning area of $5 \mu\text{m} \times 5 \mu\text{m}$ and a scanning rate of 1 Hz.

3 Results and discussion

3.1 Optical properties

Reflection versus wavelength measurements is performed at room temperature using UV–Vis spectroscopy in the range 200–1000 nm to investigate the reflection spectra. It is noticed that the effective wavelength ranges are found between 820 and 1000 nm as shown in Fig. 1. The lowest reflectance for with ultrasonic samples is at 0.6 M which ranging between 23 and 44 %, while the highest reflectance is at 1 M and it is ranging between 30 and 79 %. On the other side, lowest reflectance for without ultrasonic samples is at 0.6 M which ranging between 20 and 45 %, while the highest reflectance is at 1 M and it is ranging between 30 and 72 %. One main observation can be extracted from Fig. 1 that 0.6 M is the best Cu concentration in terms of low reflectance and high absorption for both with and without ultrasonic. It is worth mentioning that the silicon substrate able to reflect light but not absorb it or transmit it, and hence, reflection measurements have been utilized.

According to Tauc formula [19] for direct band gap semiconductors, the energy band gap of Cu₂CdSnS₄ quaternary alloy nanostructures can be estimated using the following formula:

$$(\alpha h\nu)^2 = A(h\nu - E_g) \quad (3)$$

where α is the absorption coefficient, A is a constant, E_g is the energy band gap, ν is incident photon frequency and h is the Planck's constant.

The energy band gap is estimated from absorption spectra $(\alpha h\nu)^2$ versus $h\nu$ by extrapolating the straight line portion of the curve to zero absorption coefficient as shown in Fig. 2. It is worth mentioning that the absorption spectra

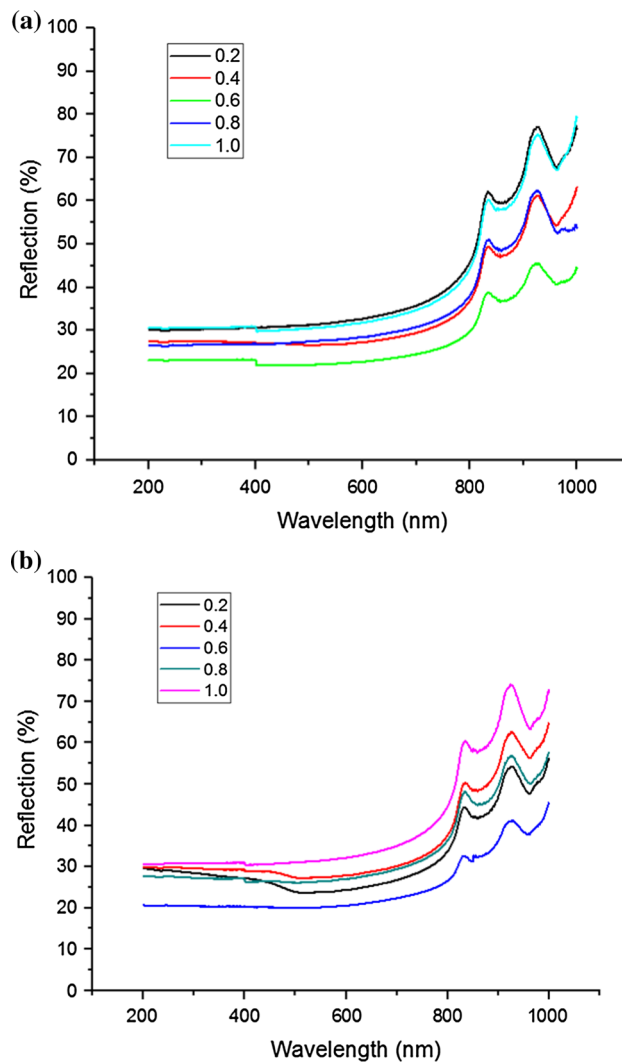


Fig. 1 Reflection (%) spectra of Cu₂CdsnS₄ quaternary alloy nanostructures deposited on *n*-Si substrates **a** with ultrasonic and **b** without ultrasonic

demonstrate many peaks and this is due to using multiple elements in preparing the solution in addition to the silicon substrate. To discuss the findings of UV–Vis measurements starting with ultrasonic samples, E_g at 0.2 M is 1.265 eV, it is dropped to 1.26 eV with increasing copper concentration to 0.4 M and another drop to 1.255 eV at 0.6 M. Suddenly, it is increased to 1.28 eV at 0.8 M but it is dropped again to 1.27 eV at 1 M, whereas energy band gap values for without ultrasonic samples starts with 1.27 eV at 0.2 M and dropped slightly to 1.265 eV with increasing copper concentration to 0.4 M, followed by a drop to 1.25 eV at 0.6 M then increased to 1.26 eV with increasing copper concentration to 0.8 M. Lastly, it is increased again to 1.275 eV at 1 M. It is observed that the trends of energy band gaps for both with and without ultrasonic samples are almost similar, the energy band gap is decreased with

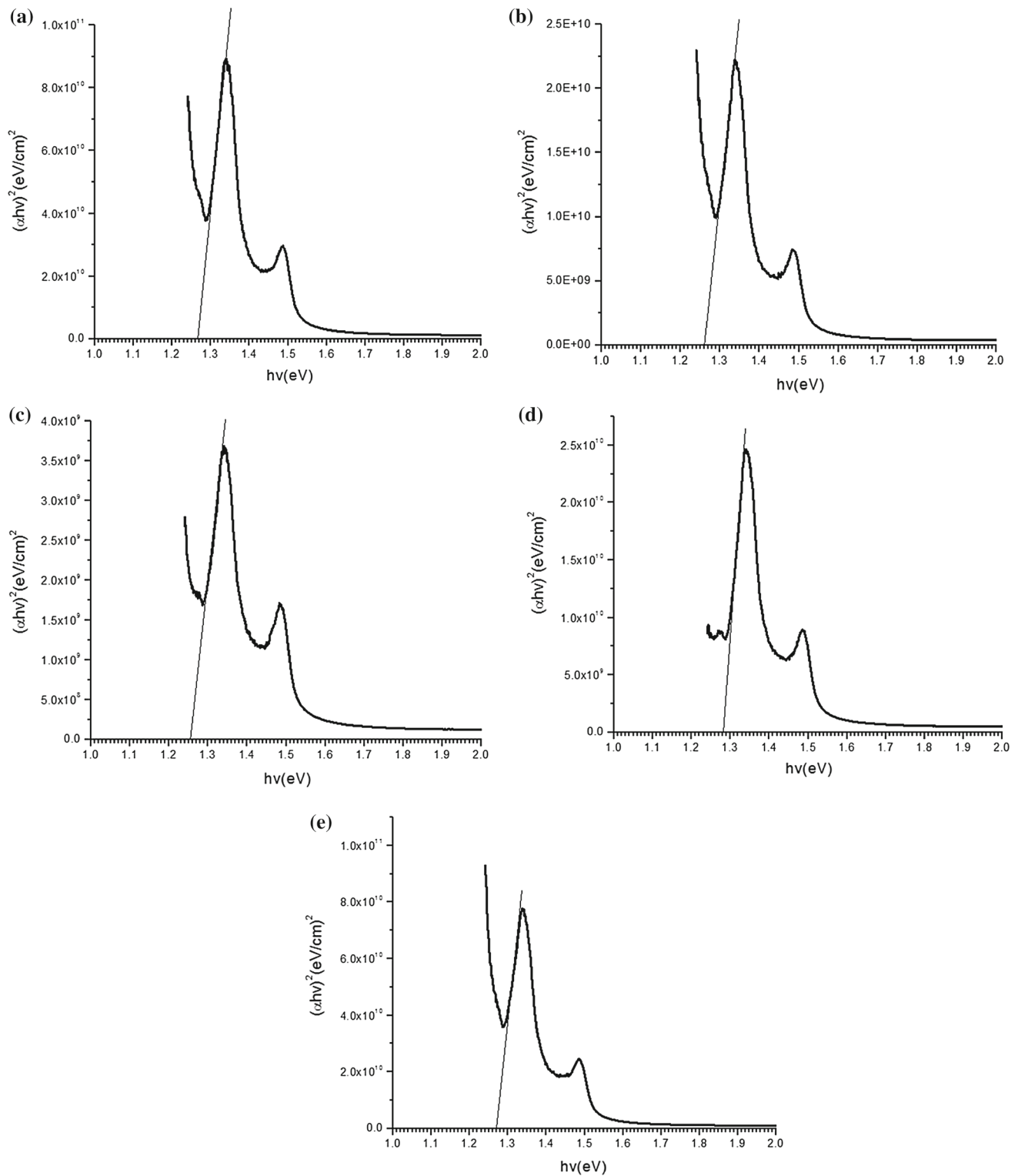


Fig. 2 $(\alpha hv)^2$ versus $h\nu$ of $\text{Cu}_2\text{CdSnS}_4$ quaternary alloy nanostructures deposited on n -Si substrates with ultrasonic at **a** 0.2 M, **b** 0.4 M, **c** 0.6 M, **d** 0.8 M, **e** 1 M and without ultrasonic at **f** 0.2 M, **g** 0.4 M, **h** 0.6 M, **i** 0.8 M, **j** 1 M

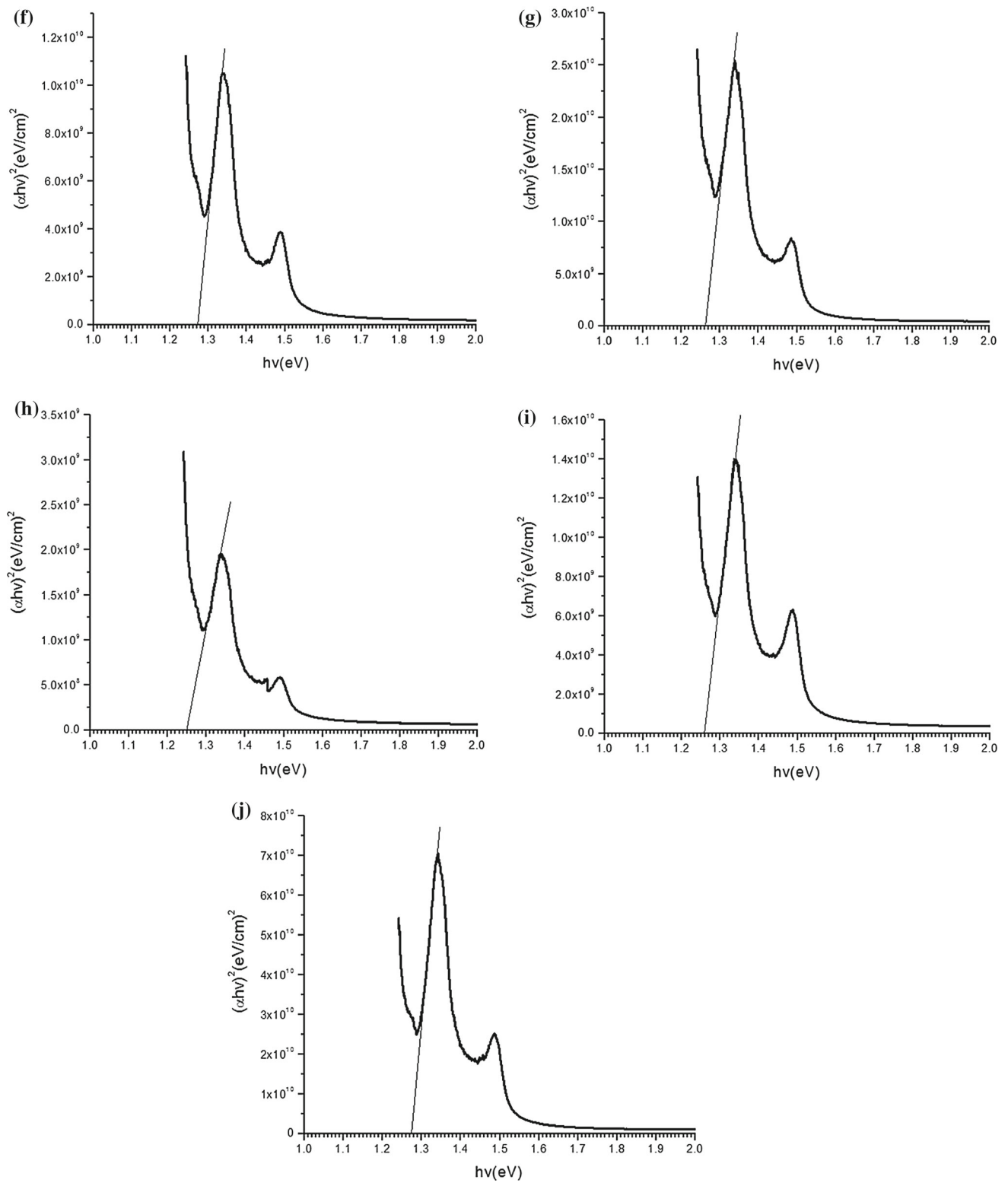


Fig. 2 continued

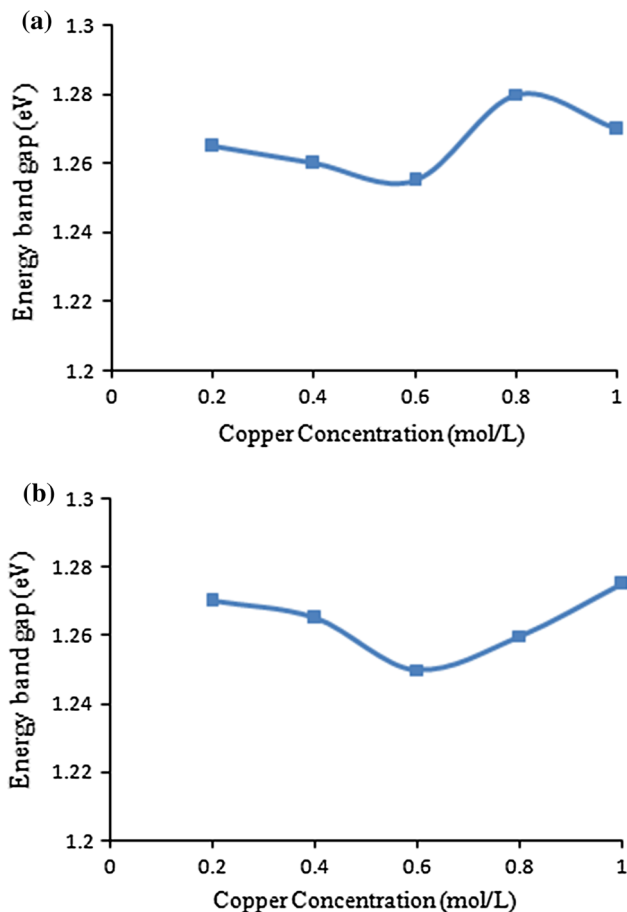


Fig. 3 Fitted UV–Vis plots of energy band gap of Cu₂CdSnS₄ quaternary alloy nanostructures as a function of copper concentration **a** with ultrasonic and **b** without ultrasonic

increasing the concentration of copper and this is in accordance with the literature [20]. Band gaps variation with copper concentration is illustrated in Fig. 3.

The PL spectra of Cu₂CdSnS₄ quaternary alloy nanostructures are shown in Fig. 4. For with ultrasonic, the E_g at 0.2 M is 1.58 eV, dropped to 1.56 eV with increasing the copper concentration to 0.4 M and another drop to 1.53 eV at 0.6 M. It is increased to 1.62 eV at 0.8 M. Lastly, it is dropped to 1.6 eV at 1 M, whereas for without ultrasonic, E_g starts with 1.57 eV at 0.2 M, then dropped to 1.56 and 1.52 eV with increasing copper concentration to 0.4 and 0.6 M, respectively, then increased to 1.54 eV at 0.8 M and continued to 1.58 eV for 1 M. It shall be noted that 0.6 M has the highest intensity for with and without ultrasonic as shown in Fig. 4.

The deduced band gaps are in a good agreement with the published data [15–19]. The band gaps are quite close to the optimum band gap required for solar cells which indicate that Cu₂CdSnS₄ quaternary alloy nanostructures are promising materials for solar cells applications. The measured energy band gaps of Cu₂CdSnS₄

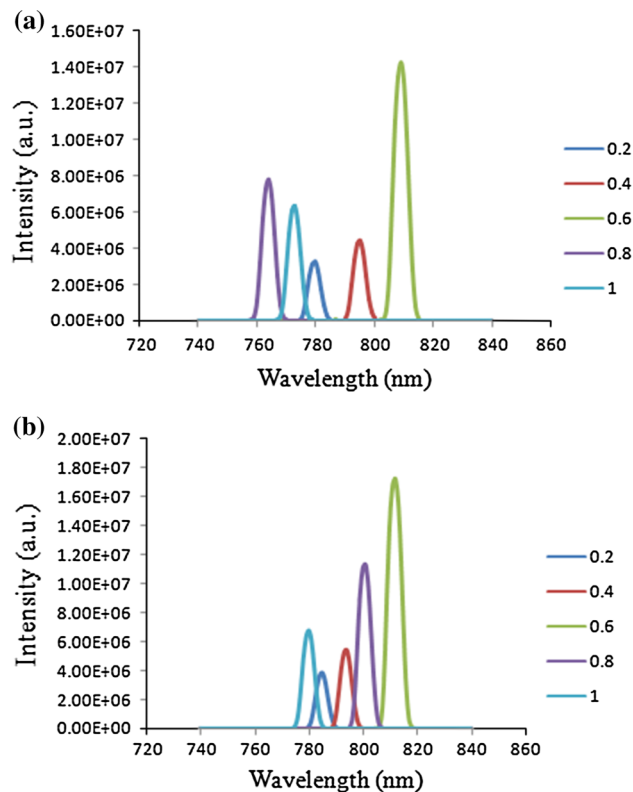


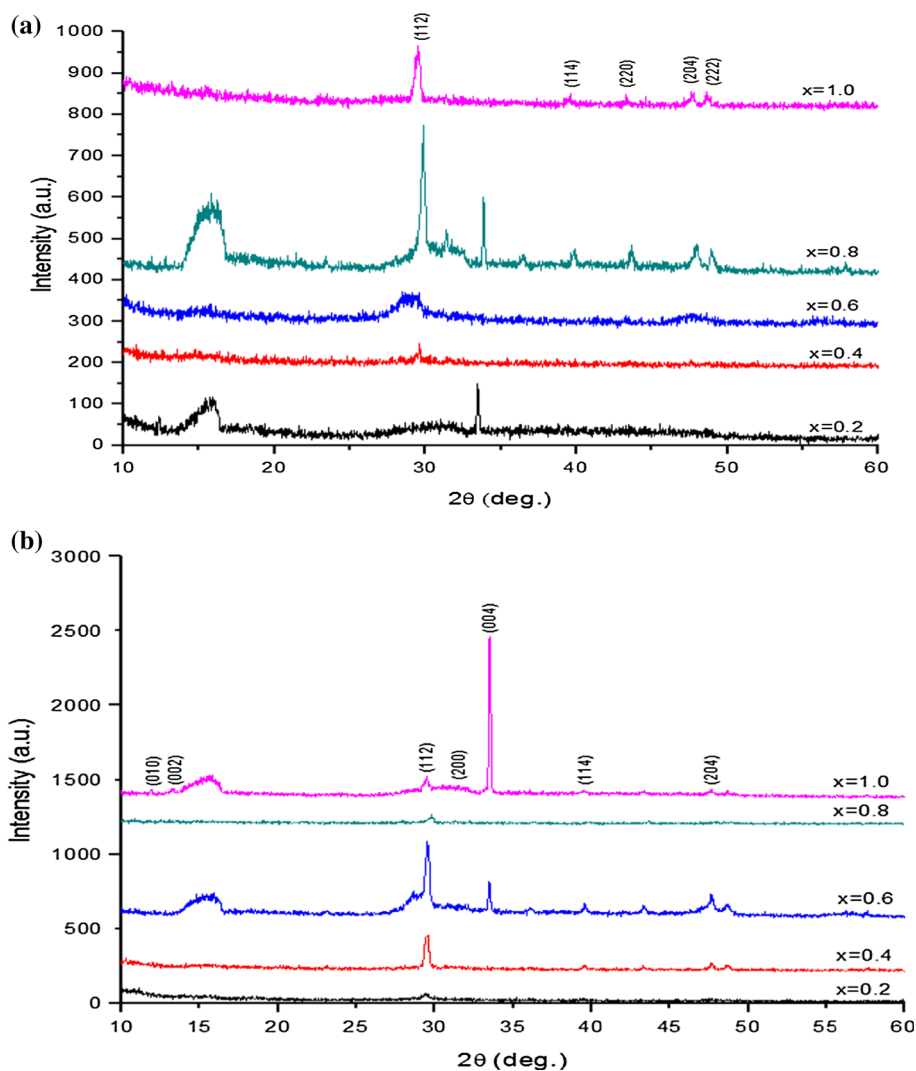
Fig. 4 PL of Cu₂CdSnS₄ quaternary alloy nanostructures as a function of copper concentration **a** with ultrasonic and **b** without ultrasonic

Table 1 Measured energy band gaps of Cu₂CdSnS₄ quaternary alloy nanostructures by using UV–Vis and PL spectroscopies at different copper concentrations

Copper concentration	With ultrasonic	Without ultrasonic
Band gap using UV–Vis (eV)		
0.2	1.265	1.27
0.4	1.26	1.265
0.6	1.255	1.25
0.8	1.28	1.26
1	1.27	1.275
Band gap using PL (eV)		
0.2	1.58	1.57
0.4	1.56	1.56
0.6	1.53	1.52
0.8	1.62	1.54
1	1.6	1.58

quaternary alloy nanostructures for UV–Vis and PL spectroscopies are given in Table 1. The difference between the energy band gaps deduced from UV–Vis and that deduced from PL is clear that is attributed to the

Fig. 5 XRD patterns of $\text{Cu}_2\text{CdSnS}_4$ quaternary alloy nanostructures as a function of copper concentration **a** with ultrasonic and **b** without ultrasonic



difference between the used instruments in both cases and ambient circumstances.

3.2 Structural properties

The $\text{Cu}_2\text{CdSnS}_4$ (CCTS) quaternary alloy nanostructures have been investigated by X-ray diffraction (XRD) as shown in Fig. 5. XRD patterns provided information about the crystalline structure of the nanoparticles as well as the crystallite size. By studying with ultrasonic patterns (Fig. 5a), the CCTS nanostructures deposited at 0.2 M have three major diffraction peaks appeared at $2\theta = 12.3525^\circ$, 16.1778° and 33.4631° were attributed to (010), (002) and (004) planes, respectively, while the CCTS nanostructures deposited at 0.4 M have two major diffraction peaks appeared at $2\theta = 10.5102^\circ$ and 29.5513° were attributed to (010) and (112) planes,

respectively, and whereas the CCTS nanostructures deposited at 0.6 M have one major diffraction peak appeared at $2\theta = 29.4817^\circ$ was attributed to (112) plane. Also, the CCTS nanostructures deposited at 0.8 M have ten major diffraction peaks appeared at $2\theta = 16.3054^\circ$, 29.8463° , 31.4023° , 33.8285° , 36.4505° , 39.8351° , 43.6715° , 47.9921° , 48.9813° and 57.8588° were attributed to (002), (112), (200), (004), (202), (114), (220), (204), (222) and (224) planes, respectively. Lastly, the CCTS nanostructures deposited at 1 M have five major diffraction peaks appeared at $2\theta = 29.5706^\circ$, 39.5544° , 43.3667° , 47.8236° and 48.7124° were attributed to (112), (114), (220), (204) and (222) planes, respectively.

On the other side, to investigate XRD patterns for without ultrasonic in Fig. 5b, the CCTS nanostructures deposited at 0.2 M have one major diffraction peak

appeared at $2\theta = 29.4494^\circ$ was attributed to (112) plane, while the CCTS nanostructures deposited at 0.4 M have seven major diffraction peaks appeared at $2\theta = 10.2796^\circ$, 29.5127° , 36.0167° , 39.5702° , 43.3094° , 47.6533° and 48.7819° were attributed to (010), (112), (202), (114), (220), (204) and (222) planes, respectively, and whereas the CCTS nanostructures deposited at 0.6 M have ten major diffraction peaks appeared at $2\theta = 10.5476^\circ$, 16.2091° , 28.5227° , 29.563° , 33.482° , 36.1737° , 39.6078° , 43.3125° , 47.6706° and 48.695° were attributed to (010), (002), (110), (112), (004), (202), (114), (220), (204) and (222) planes, respectively. Also, the CCTS nanostructures deposited at 0.8 M have two major diffraction peaks appeared at $2\theta = 29.7836^\circ$ and 39.8248° were attributed to (112) and (114) planes, respectively. Lastly, the CCTS nanostructures deposited at 1 M have seven major diffraction peaks appeared at $2\theta = 11.8573^\circ$, 13.2451° , 29.4933° , 31.6776° , 33.4843° , 39.5094° and 47.6194° were attributed to (010), (002), (112), (200), (004), (114) and (204) planes, respectively. All the mentioned peaks are matched with the tetragonal stannite structure of $\text{Cu}_2\text{-CdSnS}_4$ that corresponding to the standard (ICDD PDF2008, 00-029-0537). It is noticed that the main peak is at (112) plane for both cases. Also, it is observed the

existence of more peaks in without ultrasonic patterns than that with ultrasonic due to the differences in electrons velocity.

The lattice constants a and c were calculated from XRD patterns of the (112) plane, using the given equations according to the tetragonal crystal system. Table 2 displays the values of a and c along with other structural parameters at different copper concentrations for with and without ultrasonic.

The inter-planer distance (d) was calculated using Bragg's law [21],

$$d = \frac{n\lambda}{2 \sin(\theta)} \quad (4)$$

where λ is wavelength of XRD using ($\lambda = 1.5406 \text{ \AA}$), and θ is the Bragg's angle.

Lattice constants a and c for tetragonal system were calculated from XRD patterns using the formula below,

$$\frac{1}{d^2} = \frac{h^2 + k^2}{a^2} + \frac{l^2}{c^2} \quad (5)$$

where hkl is Miller indices, and a and c are the lattice constants. By combining Eqs. (4) and (5), a and c can be calculated in terms of $\sin \theta$:

Table 2 Structural parameters of $\text{Cu}_2\text{CdSnS}_4$ quaternary alloy nanostructures using XRD at different copper concentrations

Cu (M)	2θ	Particle size (D) (nm)	Full width at half maximum (FWHM)	Miller indices (hkl)	Inter-planer distance (d) \AA	Lattice constants (a and c) \AA	Strain (ϵ)	Dislocation density (δ) (10^{14} lines/ m^2)	Number of crystallites particles/area (N)($\times 10^{15}$)	Thickness (t) (nm)
With ultrasonic										
0.2	29.38	54.48	0.15744	112	3.04	$a = 5.26,$ $c = 10.52$	0.038	3.368	0.408	65.95
0.4	29.55	27.25	0.3149	112	3.02	$a = 5.23,$ $c = 10.47$	0.076	13.464	2.31	46.84
0.6	29.48	14.89	0.576	112	3.03	$a = 5.24,$ $c = 10.48$	0.139	45.063	18.5	61.05
0.8	29.84	43.63	0.1968	112	2.99	$a = 5.18,$ $c = 10.37$	0.047	5.251	1.18	97.98
1	29.57	36.33	0.2362	112	3.02	$a = 5.23,$ $c = 10.46$	0.057	7.574	2.32	111.35
Without ultrasonic										
0.2	29.44	17.87	0.48	112	3.03	$a = 5.25,$ $c = 10.5$	0.116	31.3	5.08	29.03
0.4	29.51	31.14	0.2755	112	3.03	$a = 5.24,$ $c = 10.48$	0.066	10.3	0.359	10.86
0.6	29.56	62.28	0.1378	112	3.02	$a = 5.23,$ $c = 10.46$	0.033	2.58	0.082	19.81
0.8	29.78	21.81	0.3936	112	3.00	$a = 5.19,$ $c = 10.39$	0.095	21	6.5	67.48
1	29.49	27.25	0.3149	112	3.03	$a = 5.24,$ $c = 10.49$	0.076	13.5	1.41	28.6

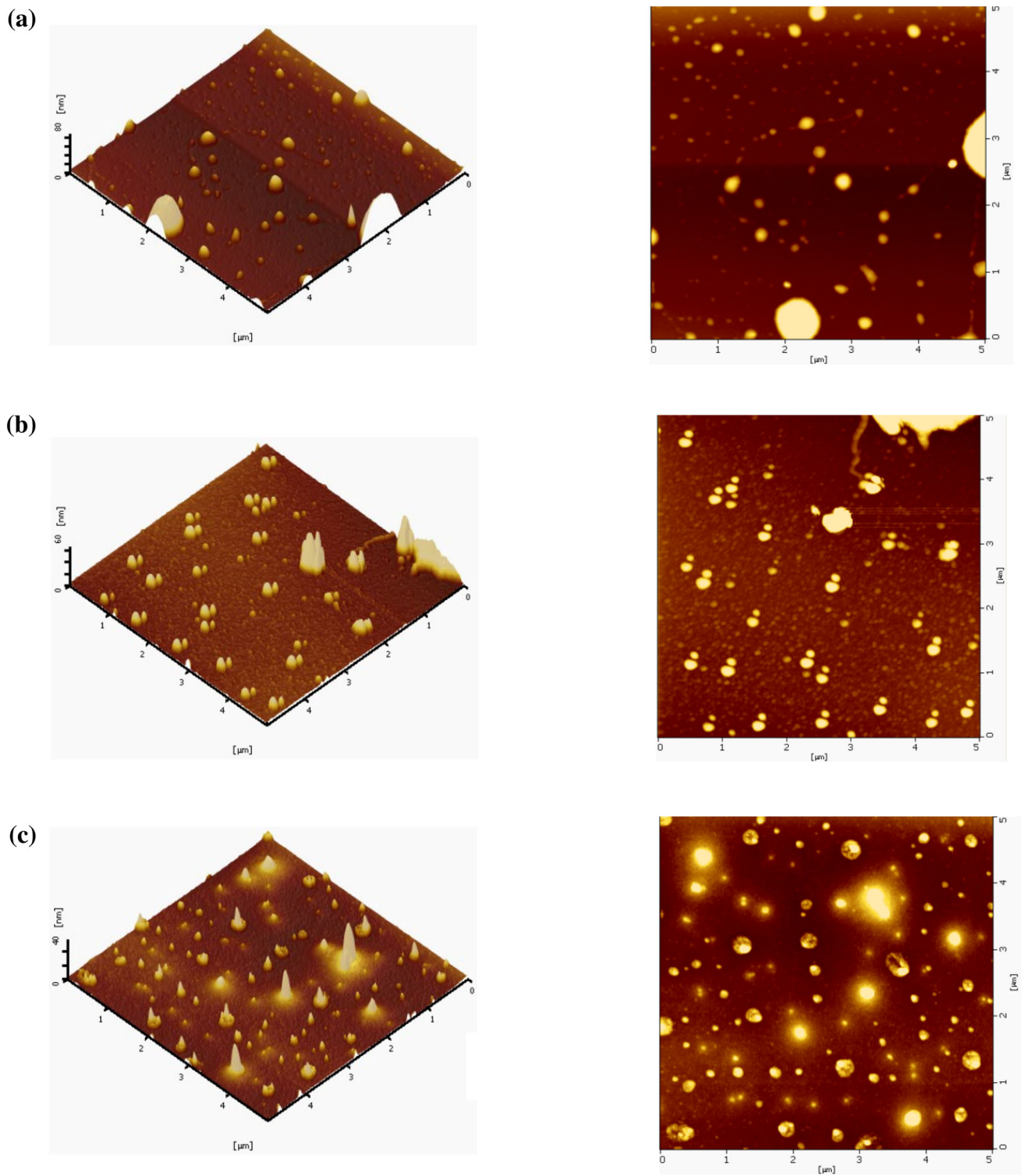


Fig. 6 3D and 2D AFM images of $\text{Cu}_2\text{CdSnS}_4$ quaternary alloy nanostructures deposited on n-Si substrates with ultrasonic at **a** 0.2 M, **b** 0.4 M, **c** 0.6 M, **d** 0.8 M, **e** 1 M and without ultrasonic at **f** 0.2 M, **g** 0.4 M, **h** 0.6 M, **i** 0.8 M, **j** 1 M

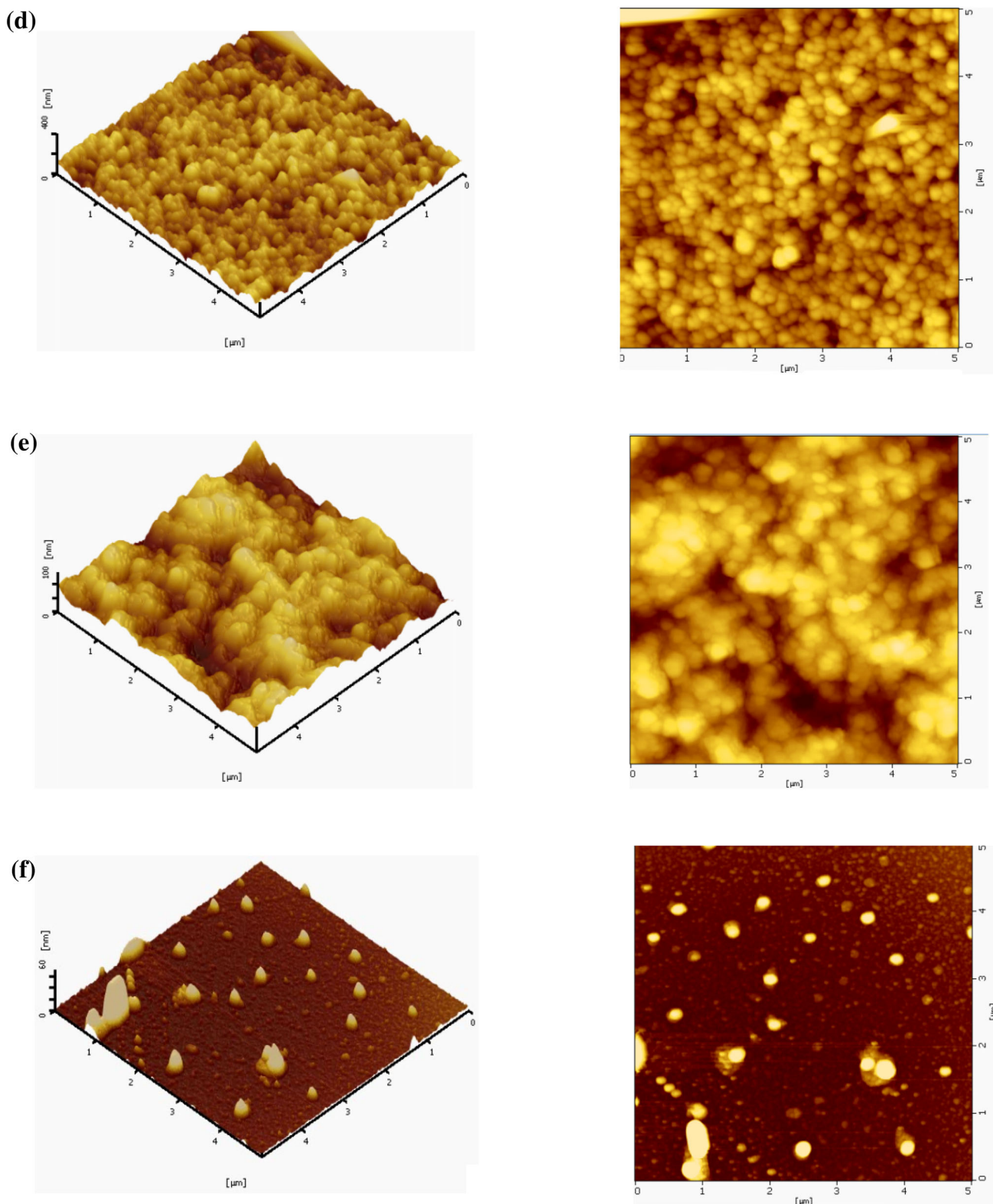


Fig. 6 continued

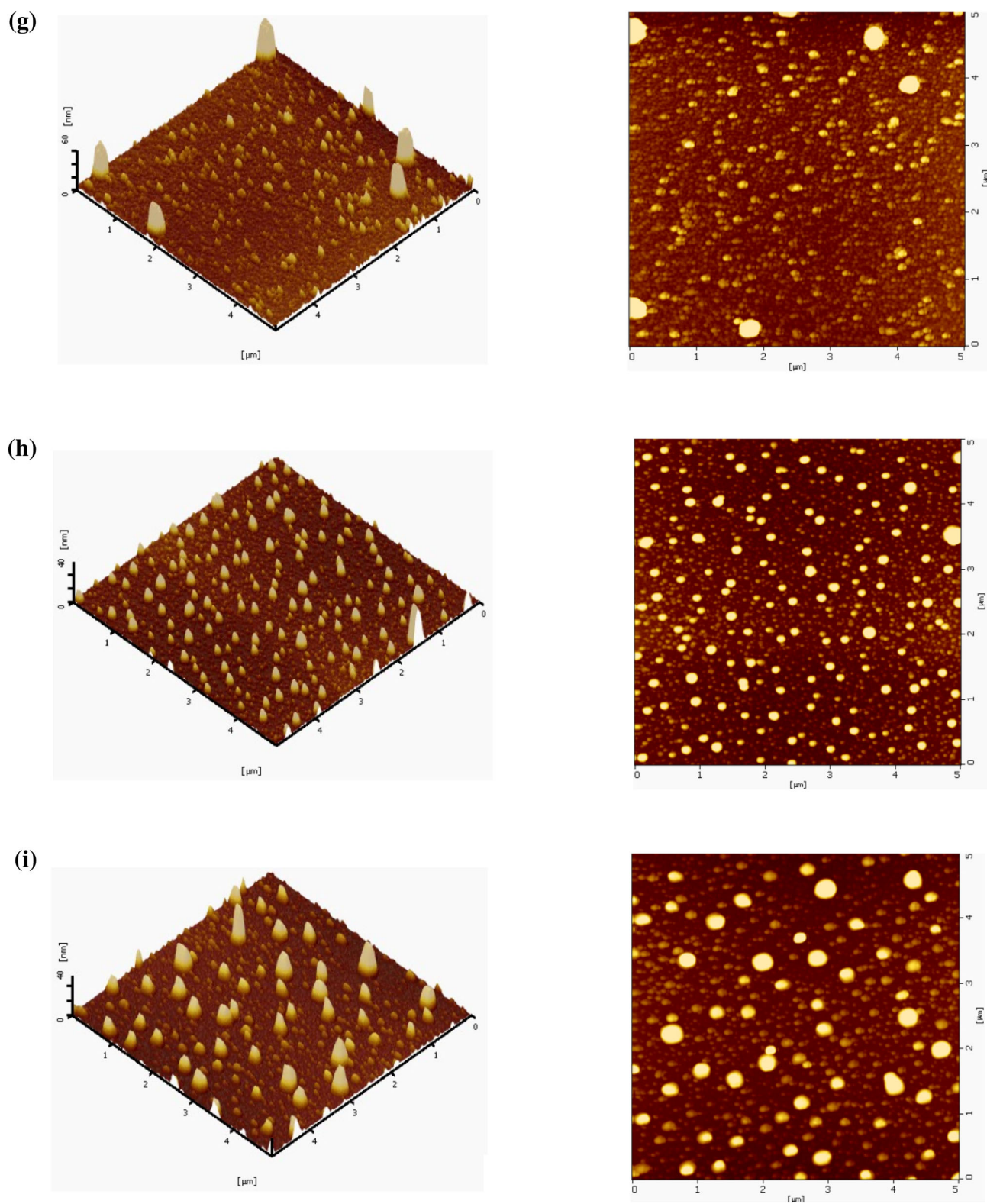


Fig. 6 continued

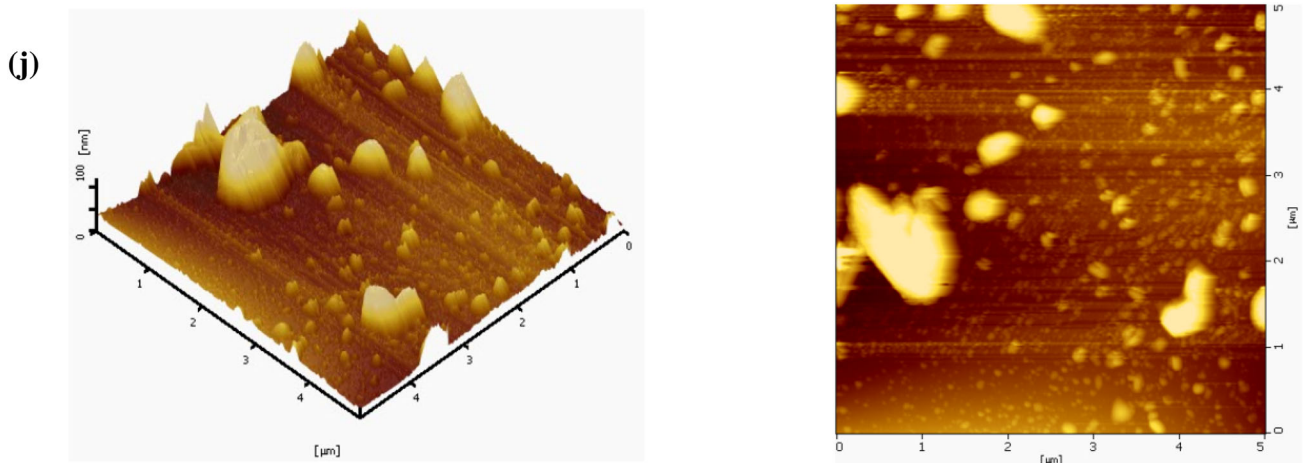


Fig. 6 continued

$$\sin^2 \theta = \frac{\lambda^2}{4a^2} (h^2 + k^2) + \frac{\lambda^2}{4c^2} (l^2) \quad (6)$$

The crystallite size (D) was calculated by Scherrer's formula [22],

$$D = \frac{k\lambda}{\beta \cos(\theta)} \quad (7)$$

where k is a constant, taken to be 0.94, and β is the full width at half maximum (FWHM) of the diffraction peak in radian. The dislocation density (δ), strain (ε) and number of crystallites per unit area (N) for (112) plane are given in Table 2. These parameters are calculated by the following equations:

$$\delta = \frac{1}{D^2} \quad (8)$$

$$\varepsilon = \frac{\beta \cos \theta}{4} \quad (9)$$

$$N = \frac{t}{D^3} \quad (10)$$

where t is the thickness as indicated in Table 2.

3.3 Topographical studies

The surface topography of $\text{Cu}_2\text{CdSnS}_4$ quaternary alloy nanostructures have been characterized, and Fig. 6 shows

Table 3 Roughness of $\text{Cu}_2\text{CdSnS}_4$ quaternary alloy nanostructures using AFM at different copper concentrations

Cu (M)	Roughness (with ultrasonic) (nm)	Roughness (without ultrasonic) (nm)
0.2	3.4	2.35
0.4	2.64	2.2
0.6	1.95	2.14
0.8	11.14	2.4
1	17.1	2.95

the AFM images at different copper concentrations: 0.2, 0.4, 0.6, 0.8 and 1 M, with and without using ultrasonic. The 2D and 3D images show the topography of $5 \mu\text{m} \times 5 \mu\text{m}$ area with 1 Hz scan rate. The surface roughness is related to many parameters such as quaternary alloy diffusion, type of substrate, annealing temperature and spin coating speed. As given in Table 3, the roughness starts with 3.4 nm at 0.2 M for with ultrasonic samples and continued to decrease with increasing the concentration until 1.95 nm at 0.6 M, the roughness increased suddenly to 11.14 nm at 0.8 M and end up with 17.1 nm at 1 M, whereas the roughness starts with 2.35 nm at 0.2 M for without ultrasonic samples and continued to decrease with increasing the concentration up to 2.14 nm at 0.6 M, then increased to 2.4 nm at 0.8 M followed by another increase

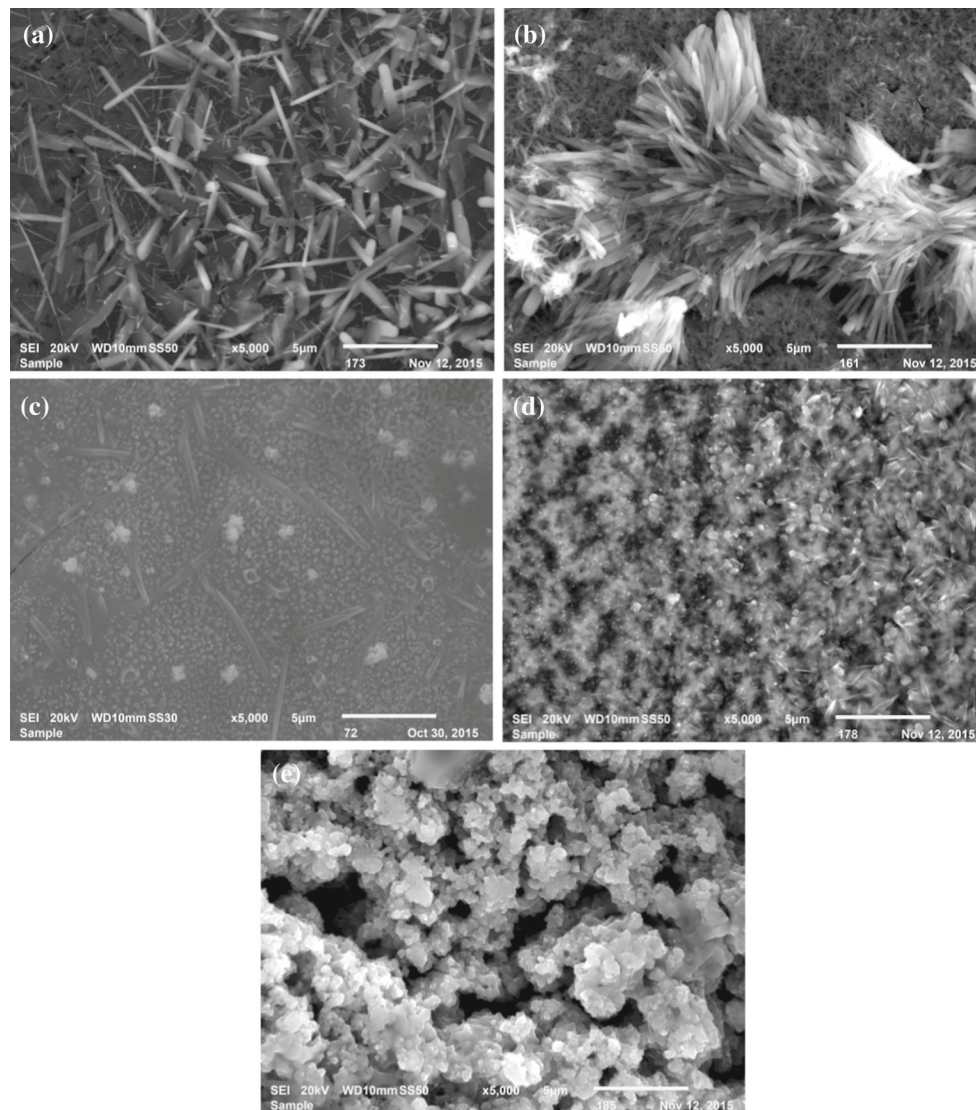


Fig. 7 SEM images of $\text{Cu}_2\text{CdSnS}_4$ quaternary alloy nanostructures deposited at different copper concentrations with ultrasonic at **a** 0.2 M, **b** 0.4 M, **c** 0.6 M, **d** 0.8 M, **e** 1 M and without ultrasonic at **f** 0.2 M, **g** 0.4 M, **h** 0.6 M, **i** 0.8 M, **j** 1 M

to 2.95 nm at 1 M. It is worth mentioning that the roughness is minimum at 0.6 M and maximum at 1 M for both, with and without ultrasonic.

3.4 Morphological studies

The SEM images show the surface morphologies of $\text{Cu}_2\text{CdSnS}_4$ quaternary alloy nanostructures deposited at different copper concentrations in Fig. 7, with and without ultrasonic in the deposition process. A closer look at these

images shows that the deposition at 0.2 and 0.4 M resulted into needle scattered shape structure. Moreover, small cracks can be seen at 0.4 M image. However, with increasing the copper concentration to 0.6 M, the morphology becomes more dense, uniform with some grains. The morphology starts to conglomerate with increasing the concentration to 0.8 M and the structure continued to accumulate until becomes ossified as observed in Fig. 7e, j. Therefore, the morphology at 0.6 M is the best for both, with and without ultrasonic.

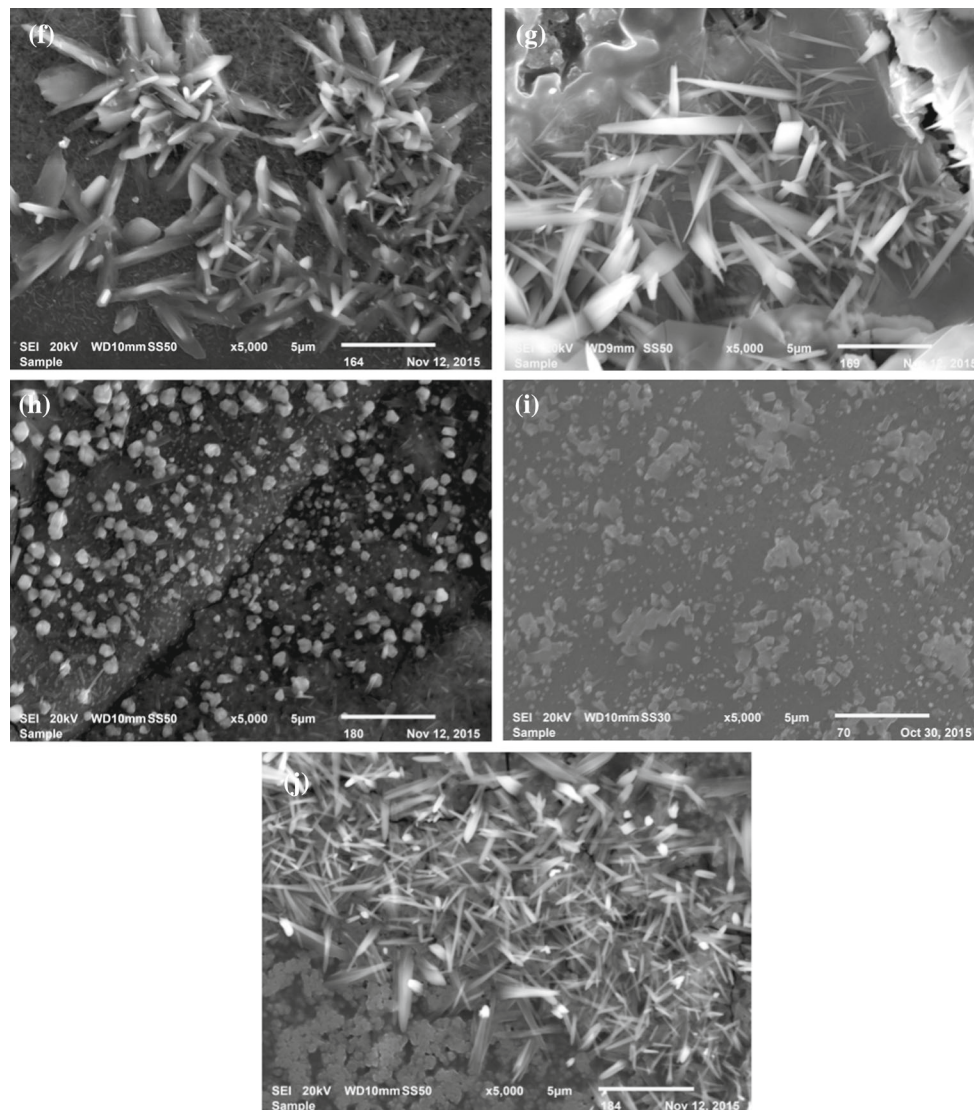


Fig. 7 continued

4 Conclusions

$\text{Cu}_2\text{CdSnS}_4$ quaternary alloy nanostructures were successfully synthesized and deposited on *n*-Si substrates via spin coating technique with annealing temperature of 300 °C at different copper concentrations (0.2–1 M), with and without ultrasonic. UV–Vis and PL measurements demonstrate that energy band gaps are 1.25–1.28 and 1.52–1.6 eV, respectively, which are quite close to the optimum band gap required for solar cells applications, and 0.6 M has the highest intensity in PL measurements. XRD results revealed the existence of more peaks in without ultrasonic samples than that in with ultrasonic, and XRD pattern at 0.6 M for without ultrasonic has ten peaks and the highest crystallite size. It is worth mentioning that the measured

lattice constants decrease with increasing copper concentration. The morphological and topographical studies indicated the superiority of 0.6 M than the other copper concentrations as shown in AFM and SEM images. These results indicated that $\text{Cu}_2\text{CdSnS}_4$ quaternary alloy nanostructures prepared using copper concentration at 0.6 M and without ultrasonic are the potential absorbing layer for cost-effective solar cells.

References

1. H. Matsushita, T. Maeda, A. Katsui, T. Takizawa, Thermal analysis and synthesis from the melts of Cu-based quaternary compounds Cu-III-IV-VI_4 and $\text{Cu}_2\text{-II-IV-VI}_4$ (II = Zn, Cd; III = Ga, In; IV = Ge, Sn; VI = Se). *J. Cryst. Growth* **208**, 416–422 (2000)

- H. Matsushita, A. Katsui, Materials design for Cu-based quaternary compounds derived from chalcopyrite-rule. *J. Phys. Chem. Solids* **66**, 1933–1936 (2005)
- M. Saidan, A.G. Albaali, E. Alasis, J.K. Kaldellis, Experimental study on the effect of dust deposition on solar photovoltaic panels in desert environment. *Renew. Energy* **92**, 499–505 (2016)
- N. Ali, A. Hussain, R. Ahmed, M.K. Wang, C. Zhao, B.U. Haq, Y.Q. Fu, Advances in nanostructured thin film materials for solar cell applications. *Renew. Sustain. Energy Rev.* **59**, 726–737 (2016)
- A. Vossier, D. Chemisana, G. Flamant, A. Dollet, Very high fluxes for concentrating photovoltaics: considerations from simple experiments and modeling. *Renew. Energy* **38**, 31–39 (2012)
- M. Petrović, V. Chellappan, S. Ramakrishna, Perovskites: solar cells and engineering applications—materials and device developments. *Sol. Energy* **122**, 678–699 (2015)
- C. Men, Z. Tian, Q. Shao, H. Zhang, Z. An, Characterization of $\text{Cu}(\text{In}, \text{Ga})\text{Se}_2$ films deposited by single-step electron beam evaporation for solar cell applications. *Appl. Surf. Sci.* **258**, 10195–10198 (2012)
- D. Zhou, H. Zhu, X. Liang, C. Zhang, Z. Li, Y. Xu, J. Chen, L. Zhang, Y. Mai, Sputtered molybdenum thin films and the application in CIGS solar cells. *Appl. Surf. Sci.* **362**, 202–209 (2015)
- L.M. Peter, Electrochemical routes to earth-abundant photovoltaics: a minireview. *Electrochem. Commun.* **50**, 88–92 (2014)
- C. Adel, B.M. Fethi, B. Brahim, Optical and electrical characterization of CIGS thin films grown by electrodeposition route. *J. Appl. Phys. A* **122**, 1–7 (2016)
- M. Graetzel, R.A.J. Janssen, D.B. Mitzi, E.H. Sargent, Materials interface engineering for solution-processed photovoltaics. *Nature* **488**, 304–312 (2012)
- T.P. Dhakal, C.Y. Peng, R.R. Tobias, R. Dasharathy, C.R. Westgate, Characterization of a CZTS thin film solar cell grown by sputtering method. *Sol. Energy* **100**, 23–30 (2014)
- X. Zhang, X. Shi, W. Ye, C. Ma, C. Wang, Electrochemical deposition of quaternary $\text{Cu}_2\text{ZnSnS}_4$ thin films as potential solar cell material. *Appl. Phys. A Mater. Sci. Process.* **94**, 381–386 (2009)
- S.A. Vanalakar, G.L. Agawane, S.W. Shin, M.P. Suryawanshi, K.V. Gurav, K.S. Jeon, P.S. Patil, C.W. Jeong, J.Y. Kim, J.H. Kim, A review on pulsed laser deposited CZTS thin films for solar cell applications. *J. Alloys Compd.* **619**, 109–121 (2015)
- Y. Cui, G. Wang, D. Pan, Synthesis and photoresponse of novel $\text{Cu}_2\text{CdSnS}_4$ semiconductor nanorods. *J. Mater. Chem.* **22**, 12471–12473 (2012)
- H. Guo, Y. Li, X. Fang, K. Zhang, J. Ding, N. Yuan, Co-sputtering deposition and optical-electrical characteristic of $\text{Cu}_2\text{-CdSnS}_4$ thin films for use in solar cells. *Mater. Lett.* **162**, 97–100 (2016)
- Z.-Y. Xiao, Y.-F. Li, B. Yao, R. Deng, Z. Ding, T. Wu, G. Yang, C.-R. Li, Z.-Y. Dong, L. Liu, L. Zhang, H.-F. Zhao, Bandgap engineering of $\text{Cu}_2\text{Cd}_x\text{Zn}_{1-x}\text{SnS}_4$ alloy for photovoltaic applications: a complementary experimental and first-principles study. *J. Appl. Phys.* **114**, 183506 (2013)
- A.S. Ibraheem, Y. Al-Douri, N.Z. Al-hazeem, U. Hashim, D. Prakash, K.D. Verma, Effect of cadmium concentration on structural, optical and electrical properties of $\text{Cu}_2\text{Zn}_{1-x}\text{Cd}_x\text{SnS}_4$ quaternary alloy nanofibres, synthesized by electrospinning technique. *J. Nanomater.* **2016**, 7314714–7314724 (2016)
- Y. Al-Douri, A.H. Reshak, Analytical investigations of CdS nanostructures for optoelectronic applications. *Optik* **126**, 5109–5114 (2015)
- H. Cao, H. Deng, W. Zhou, J. Tao, L. Chen, L. Huang, L. Sun, F. Yue, P. Yang, J. Chu, Investigation of microstructural and optical properties of $\text{Cu}(\text{In}, \text{Al})\text{Se}_2$ thin films with various copper content. *J. Alloys Compd.* **651**, 208–213 (2015)
- Y. Al-Douri, Q. Khasawneh, S. Kiwan, U. Hashim, S.B. Abd Hamid, A.H. Reshak, A. Bouhemadou, M. Ameri, R. Khenata, Structural and optical insights to enhance solar cell performance of CdS nanostructures. *Energy Convers. Manag.* **82**, 238–243 (2014)
- Y. Al-Douri, A.H. Reshak, H. Baaziz, Z. Charifi, R. Khenata, S. Ahmad, U. Hashim, An ab initio study of the electronic structure and optical properties of $\text{CdS}_{1-x}\text{Te}_x$ alloys. *Sol. Energy* **84**, 1979–1984 (2010)